A Simplified Confined-Chain Model for AB Diblock Copolymers

Eduardo Pretel, Angélique Rasmussen, and Peter Rasmussen*

IVC-SEP, Department of Chemical Engineering, Technical University of Denmark, Building 229, DK 2800 Lyngby, Denmark

John Holten-Andersen

National Environmental Research Institute, Frederiksborgvej 399, P.O. Box 358, DK 4000 Roskilde, Denmark

Received August 20, 1996; Revised Manuscript Received December 9, 1996[⊗]

ABSTRACT: A simplified confined-chain model for AB diblock copolymers in the lamellar microphase-separated state is presented. Block end-to-end distances and segment distribution functions are calculated by random flight statistics in one dimension without solving the diffusion equations as in the traditional approach. A simple expression to evaluate lamellar domain periods is obtained in terms of polymer pure density data and molecular weights. Numerical results are in close agreement with experimental data on domain sizes. A simple criterion for determining the equilibrium microdomain morphology is presented and compared with other theories and data from the literature.

1. Introduction

Melts of AB diblock copolymers comprised of incompatible block segments generally form a microdomain structure as a consequence of microphase separation of the constituent blocks. At high temperatures, A and B blocks mix homogeneously forming a randomly-mixed state, but as the temperature is decreased, they separate on a microscopic scale, forming a microphase-separated state. The latter is characterized by A- and B-rich domains separated by a diffuse boundary caused by the mixing of incompatible segments at the interface. Three main microdomain structures have been found experimentally: the lamellar structure, the hexagonally arranged cylinders, and the body-centered cubic ordered spheres. The morphology and dimension of the domains are mainly determined by the relative length of the constituent blocks. They are also influenced by the thermodynamic interactions and the temperature. When both blocks have similar lengths and densities, a flat interface occurs, and the lamellar morphology is the equilibrium morphology, since a planar boundary gives equal properties on each side of it. However, when the block lengths become appreciably different, the system prefers to form a curved interface with the large block on the convex side and the smaller one on the concave side. This change in morphology is a consequence of the system tendency of having a uniform segment density in order to keep a minimum free energy.[1] In this way, the domain formed by the minor component changes from lamellae to cylinders and, finally, to spheres when the asymmetry between the A and B blocks is increased. Other domain morphologies, as the bicontinuous microstructures, have been identified recently between the lamellae and the hexagonally arranged cylinders.[2−4]

The development of theoretical models for microphase separation in block copolymer systems began about a quarter of a century ago. Researchers have used different approaches to elaborate theories that can answer basic questions such as when microphases are formed, which morphologies are stable, and what the domain dimensions are. They have also developed models to study block copolymers in solutions with solvents, homopolymers, homopolymer blends, and other block copolymers. These models have been based mainly on two different theoretical frameworks: confined-chain theories and mean-field theories. Meier[5,6] developed the first AB diblock copolymer model based on confined chains. In his theory, the copolymer blocks are modeled by random flight chains of segments that are constrained by boundaries. These boundaries are created by the incompatibility between unlike segments and they restrict segments of the same type to segregated regions of the space. The confined-chain model has been modified to include diblock copolymer solutions with selective and nonselective solvents[7,8] and homopolymers.[9] Zielinski and Spontak[10,11] have extended the confined-chain model for $(AB)_n$ and ABC multiblock copolymers. Helfand and co-workers[12,13] developed a mean-field theory for AB diblock copolymers in which the chain statistics are obtained by a random flight approximation in the presence of a potential field. This potential field is created by the energetic interactions of the A and B segments, and it is associated with Flory's interaction parameter χ_{AB}. Ohta and Kawasaki[14] developed a mean-field theory for determining the equilibrium morphology of diblock copolymer melts based on a random phase approximation proposed initially by Leibler.[15] This theory has been extended and applied to ABC triblock copolymers by Nahazawa and Ohta[16] and Zheng and Wang.[17] A different formulation of a mean-field theory has been introduced by Semenov[18] by using an electrostatic analogy. All the theories mentioned above have been mainly used to study the equilibrium morphology of the microphase-separated state in the strong-segregation limit, where the interface thickness dividing the A-rich and B-rich domains is sufficiently small compared to the dimensions of the microstructure.

Determination of equilibrium microdomain morphologies and sizes in the previous theories requires the minimization of the system total free energy. The diblock copolymer system must attain the equilibrium morphology and microdomain size that give the minimum total free energy. In general, both determinations include the manipulation of rather complex mathemati-

[⊗] Abstract published in *Advance ACS Abstracts,* April 1, 1997.

S0024-9297(96)01261-2 CCC: $14.00 © 1997 American Chemical Society

cal formulas that may require computer calculations even for the simple lamellar microstructure.[13] Holten-Andersen[19] developed some basic ideas for a simplified confined-chain model that allows the prediction of microdomain sizes in a simple and straightforward way. His model is basically a simplification of Meier's theory and retains the physical aspects of microphase separation in the strong-segregation limit. In this work, Holten-Andersen's ideas are presented and extended to calculate domain dimensions in lamellar microstructures. A and B blocks are modeled by random flight statistics in one dimension. The number of block configurations, block end-to-end distances, and segment distribution functions are obtained for two model blocks: a free block and a restricted block. The first one represents a block in a randomly-mixed state, and the second one is an approximation to a block in a microphase-separated state. In a restricted block, the interface phenomenon is modeled by an absorbing barrier close to the place where the junction between the A and B blocks is located. The theoretical development begins with the introduction of the basic assumptions of the model. Then, the number of possible configurations is evaluated for each model block and the density distribution of segments is obtained. The latter is used to calculate domain dimensions based on a uniform segment density criteria throughout the domain microstructure. A simple expression is obtained in terms of pure polymer density data and molecular weights. This expression is used to predict lamellar periods, and the results are compared with experimental data for different diblock copolymer systems. Results show that the simplified confined-chain model provides an alternative method for calculating lamellar microdomain dimensions by using a simple approach and experimental data that can be easily found in the literature. Although this model is an approximation of an AB diblock copolymer melt, it gives meaningful and simple expressions for representing block copolymer molecules in randomly-mixed and lamellar microphase-separated states. Furthermore, it provides basic concepts for estimating the entropy loss associated with chain confinement in microdomains. Future refinement of this approach must include a more detailed model to represent the interfacial phenomenon. In the last section of this work, a criterion to determine the equilibrium microdomain morphology is derived in terms of the block volume fractions. This criterion gives accurate information on the morphology transitions, and it is compared to other theories and experimental results.

2. Chain Statistics for Free and Restricted Blocks

An AB diblock copolymer molecule in a randomly-mixed state (homogeneous solution) does not have any restrictions on the placement of its segments throughout the volume of the system. In contrast, the same molecule in a microphase-separated state does have segment placement constraints as a consequence of the repulsion of the different constituent blocks. A certain degree of mixing of unlike segments occurs at the microdomain interface, and practically no mixing at all occurs inside each A or B microdomain. The development of a simplified confined-chain model for AB diblock copolymers is based on the ideas given by Meier[5] and Holten-Andersen.[19] The basic assumptions of the model are described in the following list:

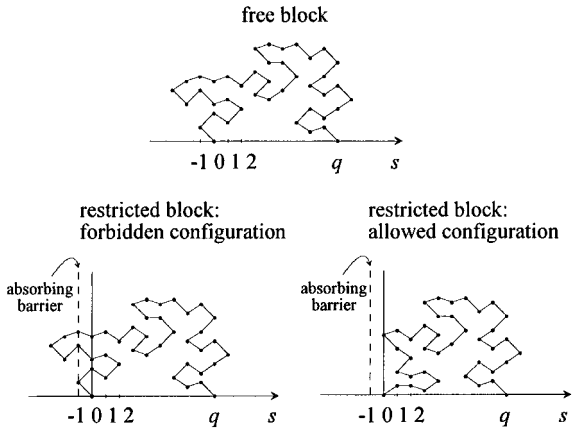

Figure 1. Free and restricted blocks.

1. Each block in the AB diblock copolymer molecule is comprised of p_i segments of length l_i (i = A, B) joined in sequence.
2. Segment distributions and block configurations are described by random flight statistics in one dimension.[20] This dimension corresponds to a projection axis of a three-dimensional chain. In a microphase-separated system, the direction of the projection axis is normal to the surface of the microdomain.
3. The interface between A and B domains is represented as an absorbing barrier which contains the junction between the two blocks. The distribution of A segments inside A-rich microdomains is independent of the distribution of B segments inside B-rich microdomains. The distributions are a direct result of the absorbing barrier condition at the interface.
4. The microdomain dimensions are only determined by the diblock copolymer conformations that give a uniform segment distribution throughout the domain.

As a consequence of the segment placement restrictions in the microphase-separated state, there is a reduction in the number of possible block configurations compared with the same number in the randomly-mixed state. By using random flight statistics in one dimension and a simple counting procedure, the number of block configurations for both states can be easily evaluated. Furthermore, the segment density distribution functions can be also obtained. In order to get the number of possible block configurations, two model blocks will be studied: a free block, equivalent to a block in a randomly-mixed state, and a restricted block, equivalent to a block in a microphase-separated state. Schematic representations of both blocks are shown in Figure 1. The main goal of the following sections is to determine the number of block configurations for the two model blocks when the distance along the projection axis and between the block end segments is x. Each segment contributes to distance x with a finite length equivalent to the projection of the segment length, l_i, on the projection axis. This length can be found statistically considering that each segment is capable of choosing any direction in the space with equal probability[20]

$$\sqrt{\overline{l_{ix}^2}} = \frac{l_i}{\sqrt{3}} \tag{1}$$

where the left-hand side of the equation is the root-mean-square of the projection of a segment on the x-axis. A nondimensional end-to-end distance q is defined as

$$q = \frac{x}{\sqrt{l_{ix}^2}} = \frac{x}{l_i/\sqrt{3}} \tag{2}$$

A. Free Block: Randomly-Mixed State. The number of configurations for a free block with p_i segments and end-to-end distance q is obtained through the following combinatorial number:

$$N(p_i,q) = \binom{p_i}{\frac{p_i - q}{2}} \tag{3}$$

Equation 3 is the result of a random walk of p_i steps in one dimension, and it has been solved by several authors in the past. In this work, an alternative procedure for obtaining eq 3 is presented in order to introduce later the effects of constraints on segment position in a restricted block.

When the end-to-end distance on the projection axis is q, segment p_i will be found at distance q from the first segment. Then, segment $(p_i - 1)$ can be found at either distance $(q - 1)$ or $(q + 1)$. Consequently, the number of block configurations, $N(p_i,q)$, can be obtained as the contribution of two $(p_i - 1)$ segment blocks with end-to-end distances $(q - 1)$ and $(q + 1)$, respectively

$$N(p_i,q) = N(p_i - 1,q - 1) + N(p_i - 1,q + 1) \tag{4}$$

Equivalently, segment $(p_i - 2)$ can be found at either distance $(q - 2)$ or q, if segment $(p_i - 1)$ is at distance $(q - 1)$, or at either distance q or $(q + 2)$, if segment $(p_i - 1)$ is at distance $(q + 1)$. If this procedure is continued, the number of possible occurrences of a given segment in a certain position is given by the binomial coefficients shown in Table 1, and the number of block configurations is given by applying eq 4 recursively r times

$$N(p_i,q) = \sum_{s=q-r}^{q+r} \binom{r}{\frac{s + r - q}{2}} N(p_i - r,s) \tag{5}$$

where $r = p_i - n$, n is the order number of the considered segment $(0 \le n \le p)$, and s is the normalized segment position on the projection axis. Equation 5 is valid for any $0 \le r \le p_i$; i.e., the study of segment locations can proceed until the order number of the considered segment, n, is zero. The combinatorial numbers in eq 5 correspond to the binomial coefficients of row r in Table 1. Furthermore, the number of configurations, $N(p_i,q)$, satisfies the following conditions:

$$N(p_i,p_i) = 1 \;\forall\; p_i \ge 0 \tag{6.1}$$

$$N(p_i,q) = N(p_i,-q) \tag{6.2}$$

$$N(p_i,q) = 0 \;\forall\; |q| > p_i \tag{6.3}$$

When $r = p_i$, eq 5 becomes

$$N(p_i,q) = \binom{p_i}{0} N(0,q - p_i) + \ldots + \binom{p_i}{(-2 + p_i - q)/2} \times N(0,-2) + \binom{p_i}{(p_i - q)/2} N(0,0) + \binom{p_i}{(2 + p_i - q)/2} \times N(0,2) + \ldots + \binom{p_i}{p_i} N(0,q + p_i) \tag{7}$$

All the terms for $s \neq 0$ are zero because they satisfy condition 6.3. Then, the number of configurations for a p_i segment block with end-to-end distance q is reduced to eq 3. If the Laplace−DeMoivre theorem[21] is applied for large values of p_i compared with the end-to-end distance q, eq 3 gives a Gaussian distribution

$$N(p_i,q) = \binom{p_i}{\frac{p_i - q}{2}} \cong \frac{2^{p_i+1}}{\sqrt{2\pi p_i}} \exp\left(-\frac{q^2}{2p_i}\right) \tag{8}$$

Equation 8 can be expressed in terms of dimensional distance x by using eq 2 and dividing by a factor 2. This factor avoids an overcounting of configurations as a consequence of considering invalid segment positions. A given segment can only occupy even (or odd) positions as can be seen in Table 1. Then

$$N(p_i,x) = \left(\frac{3}{2\pi}\right)^{1/2} \frac{2^{p_i}}{p_i^{1/2} l_i} \exp\left(-\frac{3x^2}{2p_i l_i^2}\right) \tag{9}$$

Finally, the total number of configurations for a block with p_i segments and all possible end- to-end distances, $N_T(p_i)$, can be obtained by integration of eq 9

$$N_T(p_i) = \int_{-\infty}^{\infty} N(p_i,x)\, dx = 2^{p_i} \tag{10}$$

This number corresponds to the number of configurations for a block in the randomly-mixed state when there is no restriction on the placement of segments and a block projection on one axis is considered.

B. Restricted Block: Microphase-Separated State. In the microphase-separated state, the A and B segments are segregated into their respective domains. An A block keeps most of its segments inside the A-rich domain, and the A segment forming the joint with the B block is located in the interfacial region. The same happens for a B block. As a consequence, a considerable number of conformations are lost compared with the same number in the randomly-mixed state. In order to get the number of feasible conformations for a p_i segment block (of type A or B) when there is an interface which cannot be touched or crossed by any segment, it is assumed that the interface can be represented as an absorbing barrier close to the location where the first segment is attached on the projection axis. The counting procedure presented above is used again but, in this case, disregarding all the configurations with segments that touch or cross the absorbing barrier. This is located one position to the left of the first block segment. If this segment is at $s = 0$, then the absorbing barrier is at $s = -1$, and all the positions for $s < 0$ are forbidden for segment placement. Figure 1 shows allowed and forbidden configurations for a restricted block in one dimension. The absorbing barrier condition at the interface has been discussed by DiMarzio.[22] This is a necessary assumption in order to generate conformations with equal *a priori* probability and satisfy one of the basic assumptions of statistical mechanics.

For a restricted block, Table 2 shows the binomial coefficients associated with the number of possible occurrences of a given segment in a certain position. If the free end segment is at position $s = q$, then the first segment is attached at the interface at position $s = 0$. When analyzing the possible positions for segment $n = q - p_i - 1$ $(r = q + 1)$, all the configurations with segment $n = q - p_i - 1$ at positions $s < 0$ must be

Table 1. Number of Possible Occurrences of a Given Segment in a Certain Position along the Projection Axis for a Free Block of p_i Segments and End-to-End Distance q[a]

		s											
n	r	$q-6$	$q-5$	$q-4$	$q-3$	$q-2$	$q-1$	q	$q+1$	$q+2$	$q+3$	$q+4$	$q+5$	$q+6$
p_i	0							1						
p_i-1	1						1		1					
p_i-2	2					1		2		1				
p_i-3	3				1		3		3		1			
p_i-4	4			1		4		6		4		1		
p_i-5	5		1		5		10		10		5		1	
p_i-6	6	1		6		15		20		15		6		1

[a] Key: n, segment number; s, normalized segment position; $r = p_i - n$.

Table 2. Number of Possible Occurrences of a Given Segment in a Certain Position along the Projection Axis for a Restricted Block of p_i Segments and End-to-End Distance q

		s				
n	r	-1	0	1	2	3
p_i-q+2	q-2				1	
p_i-q+1	q-1			1		$\binom{q-1}{1}$
p_i-q	q		1		$\binom{q}{1}$	
p_i-q-1	q+1			$\binom{q+1}{1}$		$\binom{q+1}{2}$
p_i-q-2	q+2		$\binom{q+1}{1}$		$\binom{q+2}{2}$	
p_i-q-3	q+3			$\binom{q+1}{1}+\binom{q+2}{2}$		$\binom{q+3}{3}$
p_i-q-4	q+4		$\binom{q+1}{1}+\binom{q+2}{2}$		$\binom{q+1}{1}+\binom{q+2}{2}+\binom{q+3}{3}$	

discarded because they cross or touch the absorbing barrier (located at $s = -1$). Consequently, all the binomial coefficients for positions $s < 0$ are zero. For $r \geq q + 2$ and $s \leq r - q - 2$, modified binomial coefficients are obtained as a result of the forbidden s positions (see gray shaded numbers in Table 2). These new coefficients are calculated by adding up the two immediate numbers in the row above. Then, the number of configurations for a restricted block with p_i segments and end-to-end distance q is obtained as

$$N^+(p_i,q) = \sum_{s=0}^{q+r}\left[\binom{r}{\frac{s+r-q}{2}} - \binom{r}{\frac{-s-2+r-q}{2}}\right] \times N^+(p_i - r,s) \quad (11)$$

Applying eq 11 for $r = p_i$, where s can only take the value 0, the following simple expression is obtained for $N^+(p_i,q)$:

$$N^+(p_i,q) = \binom{p_i}{\frac{p_i-q}{2}} - \binom{p_i}{\frac{p_i-q}{2}-1} = \frac{2(q+1)}{p_i+q+2}\binom{p_i}{\frac{p_i-q}{2}} \quad (12)$$

Equation 12 is the result of random flight statistics in one dimension for a restricted block. This result agrees with the expression obtained by DiMarzio.[22] The number of block configurations for a restricted block is reduced by a factor of $2(q + 1)/(p_i + q + 2)$ compared with the same number for a free block (eq 3). This factor is less than unity ($q \ll p_i$) and this is an important result that will be used in the following developments. For $1 \ll q \ll p_i$, eq 12 gives a Rayleigh distribution

$$N^+(p_i,q) = \frac{2(q+1)}{p_i+q+2}\binom{p_i}{\frac{p_i-q}{2}} \cong \sqrt{\frac{2}{\pi}}2^{p_i+1}\frac{q}{p_i^{3/2}}\exp\left(-\frac{q^2}{2p_i}\right) \quad (13)$$

Then, the distribution $N^+(p_i,x)$ in dimensional variable x is

$$N^+(p_i,x) = \frac{3}{(2\pi)^{1/2}}\frac{2^{p_i+1}}{p_i^{3/2}\,l_i^{2}}x\exp\left(-\frac{3x^2}{2p_i l_i^{2}}\right) \quad (14)$$

Finally, the total number of configurations for a restricted p_i segment block with all possible end-to-end distances, $N_T^+(p_i)$, can be found by integrating eq 14 from 0 to ∞

$$N_T^+(p_i) = \int_0^\infty N^+(p_i,x)\,dx = \sqrt{\frac{2}{\pi p_i}}2^{p_i} \quad (15)$$

The result of eq 15 differs by the $(2/\pi p_i)^{1/2}$ factor from that obtained in eq 10. When the projection of a block in one dimension is considered, that factor accounts for the loss of configurations of a block that changes from free to restricted space. The restricted space is created by a plane perpendicular to the projection axis. Results

of eqs 10 and 15 can be used to calculate the total number of configurations for AB diblock copolymer molecules having p_A and p_B segments. By applying those equations to both blocks, A and B,

$$N_{TAB}(p_A,p_B) = N_T(p_A)\, N_T(p_B) = 2^{p_A+p_B} \quad (16)$$

$$N_{TAB}{}^{+}(p_A,p_B) = N_T{}^{+}(p_A)\, N_T{}^{+}(p_B) = \frac{2^{p_A+p_B+1}}{\pi(p_A p_B)^{1/2}} \quad (17)$$

where $N_{TAB}(p_A,p_B)$ and $N_{TAB}{}^{+}(p_A,p_B)$ are the numbers of configurations for free and restricted AB diblock copolymer molecules, respectively.

Meier[5] identified the contributions to calculate the total free energy change associated with microphase separation from a randomly-mixed state. One of these contributions, the entropy loss caused by the segregation of segments to the microdomain regions, can be approximately calculated by using eqs 16 and 17

$$\Delta S_c = Nk \ln\frac{N_{TAB}{}^{+}(p_A,p_B)}{N_{TAB}(p_A,p_B)} = Nk \ln\frac{2}{\pi(p_A p_B)^{1/2}} \quad (18)$$

where ΔS_c only accounts for the entropy loss resulting when constraints are applied to keep the A and B segments within their respective domains.

3. Domain Size: Lamellar Microstructure

The equations obtained in the previous sections for the projection of a block in one dimension are valid for describing lamellar microstructures. In these types of microphases, there is planar symmetry and the domain sizes are determined by the segment distributions in the direction normal to the interfacial area. Segment distributions in the other two Cartesian directions do not affect the domain size because they are not restricted. A constant density distribution of segments throughout the domain will be taken as the criterion to evaluate the domain sizes. This criterion is justified by the fact that very large stresses are required to create regions of low density for highly incompressible materials. These materials will try to create any block perturbation in order to maintain a uniform density.[1]

The probability of finding the last segment of a restricted block at distance x, when all segments are at $x \geq 0$, can be found by normalization of eq 14

$$P^{+}(p_i,x) = \frac{N^{+}(p_i,x)}{\int_0^\infty N^{+}(p_i,x)\, dx} = \frac{3}{p_i l_i{}^2} x \exp\left(-\frac{3x^2}{2p_i l_i{}^2}\right) \quad (19)$$

Then, the density distribution of segments for a restricted block, $\rho^{+}(x)$, can be obtained by solving the following expression:

$$\rho^{+}(x) = \sum_{k=1}^{p_i} P^{+}(k,x) P_{x\geq 0}{}^{+}(p_i - k,x) \quad (20)$$

Here, $P_{x\geq 0}{}^{+}(p_i - k,x)$ is the probability of finding all the $p_i - k$ segments in the restricted space, $x \geq 0$, when the kth segment is at x. Hesselink[23] derived an expression for $P_{x\geq 0}{}^{+}(p_i - k,x)$. He also studied the effect of considering $P_{x\geq 0}{}^{+}(p_i - k,x) = 1$. A slightly more compressed density distribution of segments was obtained compared to the case when the correct expression for $P_{x\geq 0}{}^{+}(p_i - k,x)$ was used. No major differences in the shape of the distributions could be observed. For simplicity and based on Hesselink's results, it is assumed that the density distribution for a restricted block can be calculated by setting $P_{x\geq 0}{}^{+}(p_i - k,x) = 1$

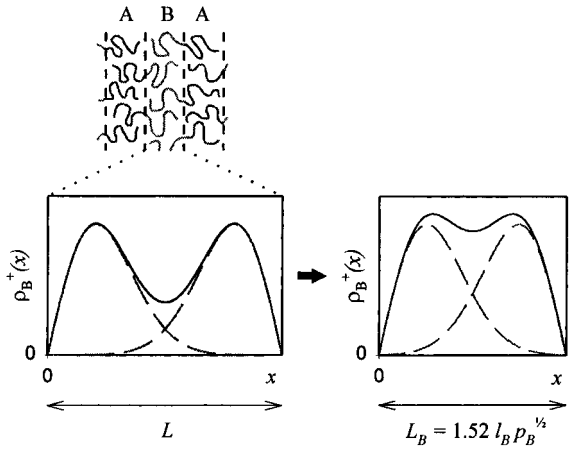

Figure 2. Density distribution of segments in a lamellar domain: dashed lines, density for each block attached to the domain borders; solid line, total density distribution.

$$\rho^{+}(x) = \sum_{k=1}^{p_i} P^{+}(k,x) = \sum_{k=1}^{p_i} \frac{3}{k l_i{}^2} x \exp\left(-\frac{3x^2}{2k l_i{}^2}\right) \quad (21)$$

Equation 21 gives the density distribution of segments as a summation of Rayleigh distributions. The summation on k can be transformed into an exponential integral as shown also by Hesselink.[23] In order to avoid the use of an exponential integral function and keep the simplicity of the expressions, the summation of Rayleigh distributions is approximated to a unique Rayleigh distribution in the following way:

$$\rho^{+}(x) \cong \frac{p_i}{a^2} x \exp\left(-\frac{x^2}{2a^2}\right) \quad (22)$$

Constant a is determined by making the second moment of the approximate distribution equal to the second moment of the distribution given by eq 21. Then, the density distribution of segments of a restricted block is given by

$$\rho^{+}(x) = \frac{6}{l_i{}^2} x \exp\left(-\frac{3x^2}{p_i l_i{}^2}\right) \quad (23)$$

If an AB diblock copolymer molecule is isolated in a very poor solvent media and, at the same time, the A and B segments repel each other sufficiently, the density distribution of segments for each block will be given by eq 23. Now, if the solvent is evaporated and the A and B blocks are about the same size, the blocks of the same type will tend to approach and form lamellar domains. In the context of this simplified theory for diblock copolymers, it is assumed that the domain size will be determined by how close two blocks of the same type can approach each other in order to keep a uniform density distribution throughout the domain. This is illustrated in Figure 2 in which a lamellar domain is represented in one dimension perpendicular to the interfacial area. The domain size is characterized by length L_i on the x axis, and one block is placed on each domain border. In order to get the domain size, the two blocks are brought closer until the distance L_i that gives

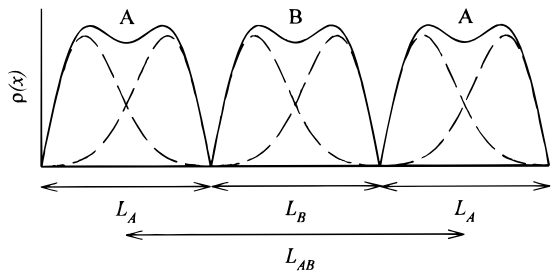

Figure 3. Lamellar microstructure in terms of the simplified confined-chain model.

the most uniform density distribution is obtained. This requirement can be approximately satisfied by the following simple condition on the total density

$$\rho_T^+(L_i/4) = \rho_T^+(L_i/2) \tag{24}$$

where $\rho_T^+(x)$ is the total density, i.e., the density obtained by adding the contributions of the two blocks. By solving condition 24, the domain length is obtained as

$$L_i = 1.52 l_i p_i^{1/2} \tag{25}$$

The total density distribution of segments for this domain length is shown in Figure 2. Equation 25 gives the domain length in terms of the unperturbed block dimension, $l_i p_i^{1/2}$. For a lamellar domain, Meier[6] obtained $L_i = 1.40\ l_i p_i^{1/2}$ by solving the diffusion equations analytically. The result of eq 25 is very close to Meier's result, considering the approximations assumed in the present simplified model.

The dimension of regular microstructures is given in terms of a characteristic length generally known as the domain period. For a lamellar microstructure of an AB diblock copolymer, the domain period is defined as the length that goes from the center of a lamella A to the center of the next lamella A (Figure 3). Equation 25 can be used to predict the lamellar period by adding the length contribution of both blocks and assuming that the interface length contribution is negligible in the strong segregation limit. Then, an approximation to the lamellar period, L_{AB}, can be calculated as

$$L_{AB} = L_A + L_B = 1.52(l_A p_A^{1/2} + l_B p_B^{1/2}) \tag{26}$$

In fact, eq 26 may overpredict the domain period because no mixing at all is considered in the interface as can be seen in Figure 3.

4. Prediction of Lamellar Periods

Prediction of lamellar periods by using eq 26 requires one physical parameter for each block: the unperturbed block dimension, $l_i p_i^{1/2}$. This parameter is available for a great variety of polymers, and it is given in terms of the polymer molecular weight and an experimentally determined constant.[24] In this work, a simpler approach is applied to calculate the unperturbed block dimension by using only pure polymer density data. Defining a segment as being a polymer repetitive unit (a monomer), the number of segments, p_i, can be calculated by

$$p_i = \frac{M_i}{m_i} \tag{27}$$

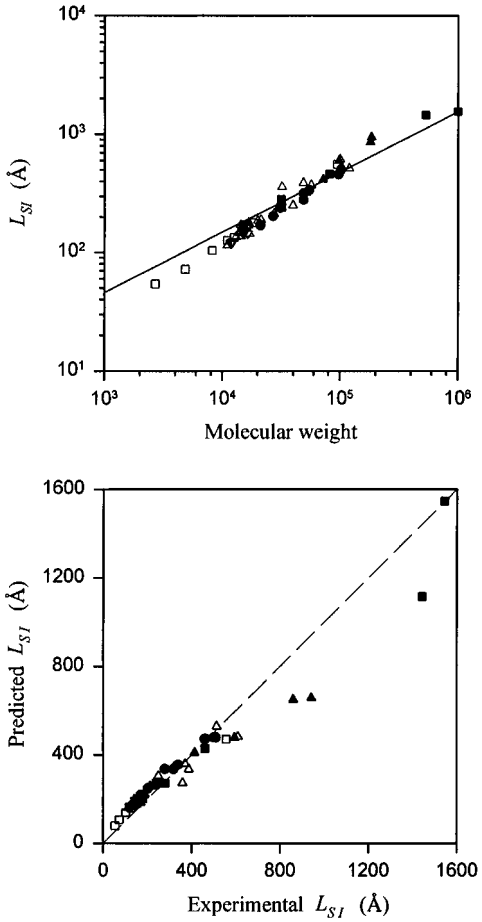

Figure 4. Predicted and experimental lamellar periods for the styrene (S)−isoprene (I) diblock copolymer. Predictions: (—). Experimental data: (●);[25] (▲);[26] (△);[27] (■);[28] (□);[29] (▼);[30] (▽).[31−50]

Table 3. Polymer Segment Lengths from Density Data and Unperturbed Dimensions

segment	$l_{i(\text{density data})}$ (Å)	$l_{i(\text{unperturbed dimensions})}$ (Å)
styrene	6.8	6.7
isoprene	6.2	6.7
butadiene	5.8	6.4
methyl methacrylate	6.5	5.8
ethylene	4.9	5.7
2-vinylpyridine	6.6	6.5

where M_i and m_i are the molecular weights of the polymer and the polymer repetitive unit (a monomer) respectively. By considering that each repetitive unit can be represented by a sphere, the volume of a segment can be obtained from pure polymer density data by

$$v_i = \frac{M_i}{\rho_i N_A p_i} = \frac{m_i}{\rho_i N_A} \tag{28}$$

where v_i is the volume of a segment, ρ_i is the density of the polymer, and N_A is Avogradro's number. Then, the length of a segment can be calculated by using the following equation:

$$l_i = \left(\frac{6}{\pi} v_s\right)^{1/3} = \left(\frac{6}{\pi} \frac{m_i}{\rho_i N_A}\right)^{1/3} \tag{29}$$

Calculated values of l_i are shown in Table 3 for some homopolymers. Finally, eqs 26, 27, and 29 can be used to predict lamellar domain periods in terms of density and molecular weight data.

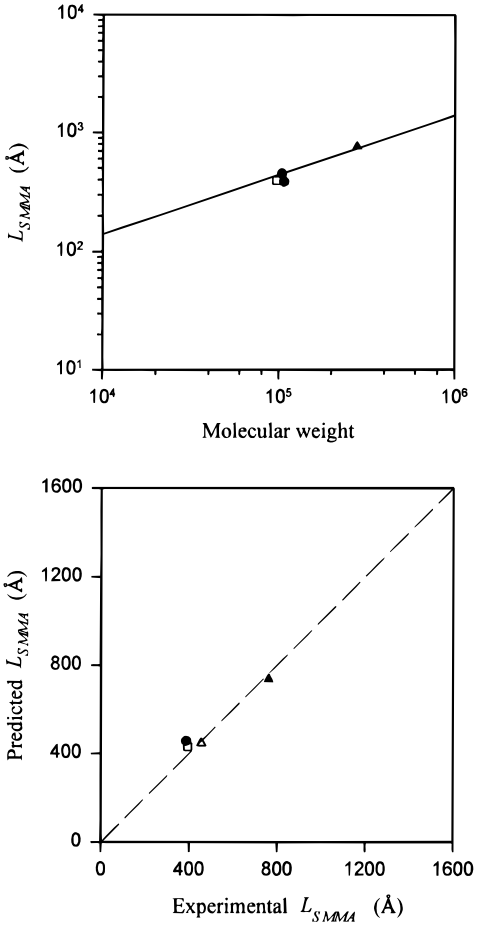

Figure 5. Predicted and experimental lamellar periods for the styrene (S)−methyl methacrylate (MMA) diblock copolymer. Predictions: (—). Experimental data: (●);[52] (▲);[53] (□).[54]

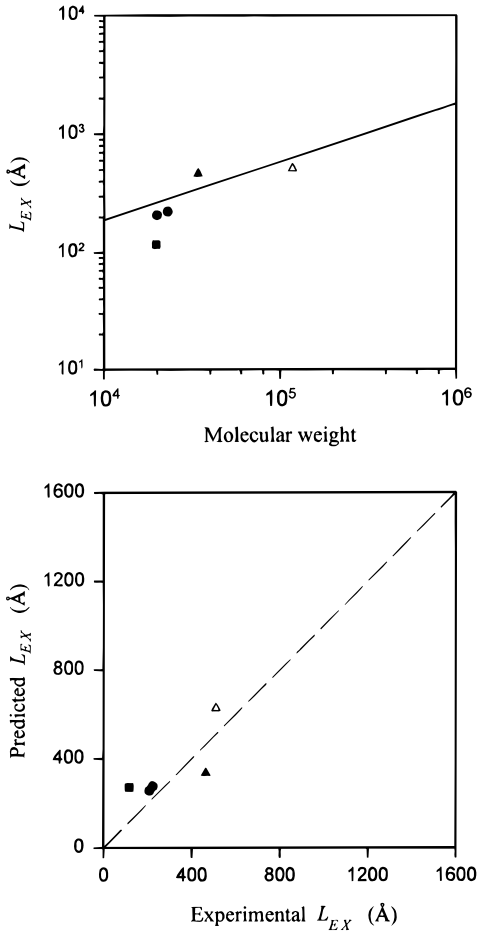

Figure 6. Predicted and experimental lamellar periods for the ethylene (E) containing diblock copolymers. Predictions: (—). Experimental data: (●),[55] X = ethylethylene; (▲),[56] X = ethylethylene; (△),[57] X = ethylpropylene; (■),[32] X = styrene.

Table 4. Predicted and Experimental Lamellar Periods for Styrene (S)−Isoprene (I) Diblock Copolymer

M_{SI}	w_S	p_S	p_I	$L_{SI-pred}$ (Å)	L_{SI-exp} (Å)	% error	ref
21 000	0.53	107	145	220	172	28	25
31 000	0.40	119	273	267	240	11	25
49 000	0.45	212	396	337	319	6	25
55 000	0.46	243	436	357	340	5	25
97 000	0.51	475	698	473	463	2	25
102 000	0.61	597	584	479	503	5	25
27 000	0.50	130	197	250	203	23	26
51 000	0.50	247	371	344	321	7	26
72 000	0.49	342	535	409	414	1	26
98 000	0.52	491	688	477	595	20	26
181 000	0.49	852	1355	649	860	25	26
185 000	0.49	862	1399	656	943	30	26
57 000	0.61	336	323	359	371	3	31
31 600	0.48	146	241	270	267	1	33
48 700	0.55	255	325	335	387	13	35
120 000	0.50	576	881	528	514	3	37
31 600	0.48	146	241	271	280	3	27
81 400	0.63	492	442	428	461	7	27
534 000	0.49	2513	3998	1115	1443	23	27
1 030 000	0.52	5143	7259	1546	1545	1	27

Several experimental techniques with angstrom-level resolution have been used to reveal the relations between microstructure and molecular parameters in microphase-separated block copolymers. Techniques such as small-angle X-ray scattering (SAXS), small-angle neutron scattering (SANS), and transmission electron microscopy (TEM) give accurate information on microdomain symmetries, periodicities, and dimensions. Experimental data from recent publications have been collected in order to compare predicted and experimentally determined lamellar periods.

The styrene−isoprene diblock copolymer has been the most studied system in the literature. Figure 4 shows a comparison between predicted and experimental results for all the data analyzed in this work for that system. Numerical values for some of the data are presented in Table 4. Prediction results are close to the experimental values in the region where most data have been obtained. However, the simplified confined-chain model cannot reproduce the correct line slope of the experimental behavior with respect to molecular weight as can be seen in Figure 4. The data lie below the predictions before the logarithm middle molecular weight range, and above them, after. The number of segments at low molecular weights (1000−10000) may not be enough to guarantee the long block requirement of the random flight approximation. Consequently, deviations as seen in Figure 4 may be expected. In the strong segregation limit, the theories of Meier,[1] Helfand and Wasserman,[13] Ohta and Kawasaki,[14] and Semenov[18] predict that the dependence of the lamellar domain period on the block copolymer molecular weight, M_{AB}, is given by

$$L_{AB} \propto M_{AB}^{2/3} \tag{30}$$

This $^2/_3$ exponential behavior has been confirmed experimentally by several authors.[25,51] For symmetric diblock copolymers ($p_A \cong p_B$), eq 26 is unable to reproduce that behavior and it gives an exponential molecular weight dependence of $^1/_2$. This is an immedi-

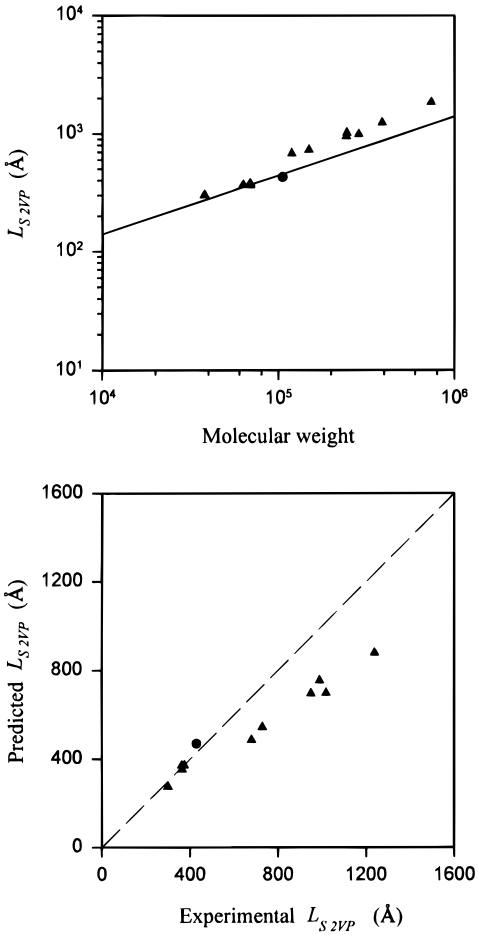

Figure 7. Predicted and experimental lamellar periods for the styrene (S)−2-vinylpyridine (2VP) diblock copolymer. Predictions: (—). Experimental data: (●);[58] (▲).[51]

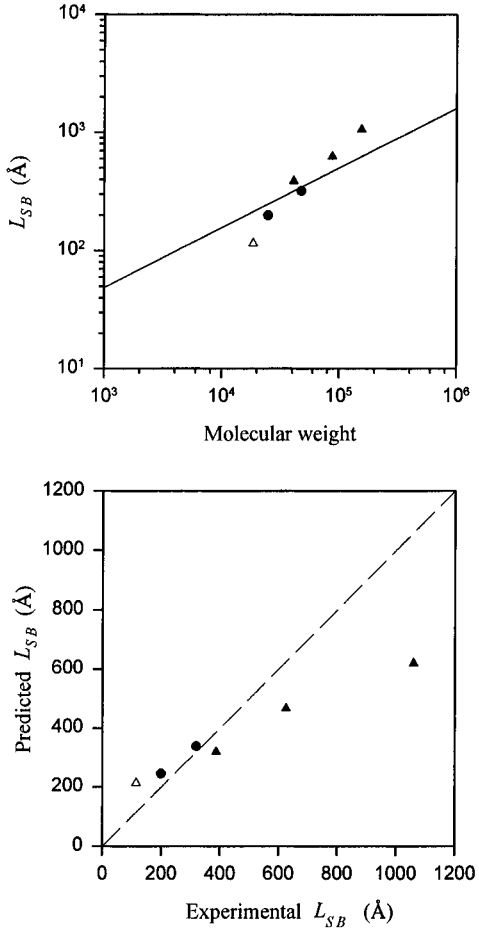

Figure 8. Predicted and experimental lamellar periods for the styrene (S)−butadiene (B) diblock copolymer. Predictions: (—). Experimental data: (●);[59] (▲):[60] (△).[32]

ate consequence of the approximations followed in the development of the simplified confined-chain model. While, in the theories mentioned above, the calculation of lamellar domain dimensions includes the minimization of the total free energy, in the present model that is done by evaluating the unperturbed block dimensions in a simple and straightforward way.

Results for other diblock copolymer systems are presented in Figures 5−8. Predictions are in good agreement with experimental data for the styrene−methyl methacrylate and the ethylene-containing diblock copolymers, as shown by Figures 5 and 6. Results are not so good for the styrene−2-vinylpyridine and the styrene−butadiene diblock copolymers (Figures 7 and 8). While the first system shows the 2/3 exponential molecular weight dependence,[51] the second system shows a different dependence that cannot be established from the scarce data shown in Figure 8. For the styrene−2-vinylpyridine system, Matsushita and coworkers[51] showed that even when the more complex theories can reproduce the experimental molecular weight dependence, the predicted and measured values of lamellar domain periods can differ by the same order of magnitude as they do in the present model.

5. Microdomain Morphology

In the previous sections, the characteristic size of lamellar microdomains has been discussed in terms of the simplified confined-chain model. In this section, the attention is focused on finding a simple criterion to determine the volume fraction range at which the lamellar microdomain morphology occurs. This criterion assumes that the thermodynamically stable state in the strong segregation limit is given by the morphology that minimizes the interfacial contact of the two incompatible segments. The interfacial contact is quantified by calculating the interfacial area contribution of a microdomain located inside a reference volume V. Figure 9 shows this situation for the three classical morphologies: lamellae, cylinders, and spheres. If f_A is the volume fraction of the minor component A, and V is a cube of volume equal to unity, the interfacial area contribution of each morphology can be calculated by

$$A_S = 4\pi R^2 = (4\pi)^{1/3}(3f_A)^{2/3} \tag{31}$$

$$A_C = 2\pi RL = \sqrt{3\pi f_A} \tag{32}$$

$$A_L = L^2 + L^2 = 2 \tag{33}$$

where A_S, A_C, and A_L are the interfacial areas of the spherical, cylindrical, and lamellar microstructures respectively, R is the radius of the sphere or the cylinder, and L is the side length of the cube ($L = 1$). In eqs 32 and 33, the ends of the cylinder and the lamella have been neglected.

Figure 10 shows the interfacial area contribution of each morphology (eqs 31−33) as a function of f_A. For $f_A > 0.5$, interfacial areas are given by the mirror image of Figure 10. Now, the most stable morphology can be predicted for the complete volume fraction range. Lamellae are predicted to be the stable morphology at medium

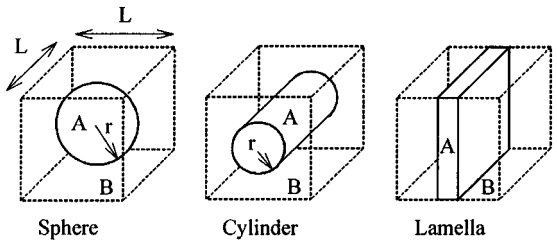

Figure 9. Spherical, cylindrical, and lamellar microdomains in a reference volume V ($L = 1$).

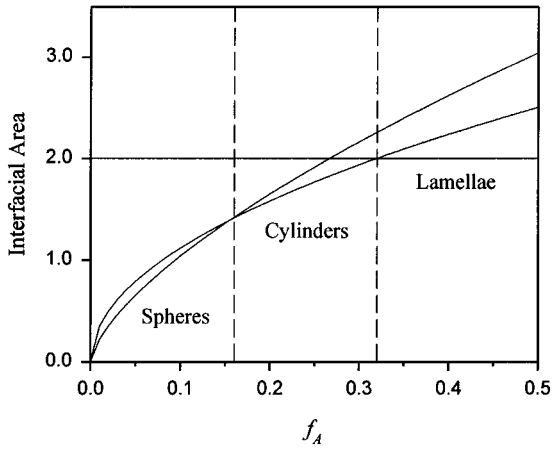

Figure 10. Interfacial areas of spherical, cylindrical, and lamellar microdomains as a function of the A-block volume fraction.

Table 5. Prediction of Morphology Transitions for Different Theories

	volume fraction, f_A	
theory	spherical/cylindrical	cylindrical/lamellar
this work	0.16	0.32
Meier	0.20	0.33
Helfand	0.10	0.33
Ohta and Kawasaki	0.22	0.36
Semenov	0.12	0.28

volume fractions ($0.32 < f_A < 0.68$), cylinders at intermediate composition ranges ($0.16 < f_A < 0.32$ and $0.68 < f_A < 0.84$), and spheres at low and high composition ranges ($f_A < 0.16$ and $f_A > 0.84$). Although the criterion presented here does not account for the more complex bicontinuous morphologies,[2−4] it easily predicts the composition ranges where the three classical microstructures can be found. A comparison between these results and previous theories is presented in Table 5. The cylindrical/lamellar change is predicted at about the same volume fraction as in previous theories. The spherical/cylindrical change is predicted at a composition that is an average of the values obtained with the other theories.

Figure 11 shows a comparison between morphology predictions and experimental data for the styrene−isoprene diblock copolymer system. The agreement is very good for all volume fractions. The morphology transitions are predicted correctly, except for the isoprene cylindrical/spherical transition at high f_A. Experiments evidence spherical microdomains at lower f_A values than predicted by the simplified criterion presented here. This disagreement can be attributed more to experimental uncertainty than to a criterion deficiency. For spherical and cylindrical microdomains, it is difficult to guarantee that experimental samples are in their thermodynamic equilibrium morphology. Diffusion barriers may preclude morphology changes and fix structures in real quasi-equilibrium states.[1]

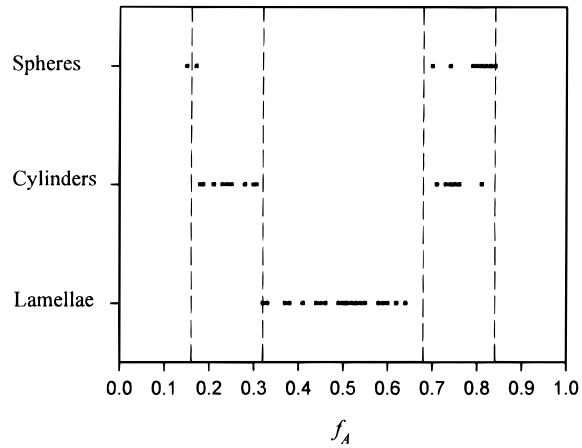

Figure 11. Morphology of some experimentally investigated styrene (S)−isoprene (I) diblock copolymers. Experimental data: (■).[27,30,34,35,39−42,44−50,61−70] Morphology transition predictions: (--).

6. Conclusions

A confined-chain model for AB diblock copolymers based on simple principles have been developed. Statistical distribution functions for blocks representing the randomly-mixed state and the microphase-separated state have been obtained by using random flight analysis in one dimension. These functions have been applied to evaluate the entropy losses caused by block segregation in lamellar microstructures and to determine lamellar domain periods. Results are in close agreement with experimental data for different AB diblock copolymer systems. Although the present theory cannot reproduce the experimental domain dimension dependence on molecular weight, it provides a simple framework to describe microphase separation and gives quantitative predictions with the same error levels as other more complex theories. Finally, a simple approach has been presented to determine the microphase morphology transitions and their region of stability.

References and Notes

(1) Meier, D. J. In *Thermoplastic Elastomers*; Legge, N. R., Holden, G., Schroeder, H. E., Eds.; Hanser Publishers: New York, 1987.
(2) Thomas, E. L.; Alward, D. B.; Kinning, D. J.; Martin, D. C.; Handlin, D. L.; Fetters, L. J. *Macromolecules* **1986**, *19*, 2197.
(3) Hamley, I. W.; Koppy, K. A.; Rosedale, J. H.; Bates, F. S.; Almdal, K.; Mortensen, K. *Macromolecules* **1993**, *26*, 5959.
(4) Schulz, M. F.; Bates, F. S.; Almdal, K.; Mortensen, K. *Phys. Rev. Lett.* **1994**, *73*, 86.
(5) Meier, D. J. *J. Poly. Sci.: Part C* **1969**, *26*, 81.
(6) Meier, D. J. *ACS Polym. Prepr.* **1970**, *11*, 434.
(7) Meier, D. J. In *Block and Graft Copolymers*; Burke, J. J., Weiss, V., Eds.; Syracuse University Press: Syracuse, NY, 1973.
(8) Meier, D. J. In *Polymer Blends and Mixtures*; Walsh, D. J., Higgins, J. S., Maconnachie, A., Eds.; NATO ASI Series; Martinus Nijhoff Publishers: Amsterdam, 1985.
(9) Kang, C. K.; Zin, W. C. *Macromolecules* **1992**, *25*, 3039.
(10) Zielinski, J. M.; Spontak, R. J. *Macromolecules* **1992**, *25*, 653.
(11) Spontak, R. J.; Zielinski, J. M. *Macromolecules* **1992**, *25*, 663.
(12) Helfand, E. *J. Chem. Phys.* **1975**, *62*, 999.
(13) Helfand, E.; Wasserman, Z. R. In *Developments in Block Copolymers. 1*; Goodman, I., Ed.; Applied Science Publishers: London, 1982.
(14) Ohta, T.; Kawasaki, K. *Macromolecules* **1986**, *19*, 2621.
(15) Leibler, L. *Macromolecules* **1980**, *13*, 1602.
(16) Nahazawa, H.; Ohta, T. *Macromolecules* **1993**, *26*, 5503.
(17) Zheng, W.; Wang, Z. G. *Macromolecules* **1995**, *28*, 7215.

(18) Semenov, A. N. *Sov. Phys. JETP* **1985**, *61*, 733.
(19) Holten-Andersen, J. Internal report, 1987.
(20) Flory, P. J. *Principles of Polymer Chemistry*; Cornell Univ. Press: Ithaca, NY, 1953.
(21) Feller, W. *An Introduction to Probability Theory an Its Applications*; John Wiley & Sons, Inc.: New York, 1966.
(22) DiMarzio, E. A. *J. Chem. Phys.* **1965**, *42*, 2101.
(23) Hesselink, F. T. *J. Chem. Phys.* **1969**, *73*, 3488.
(24) Brandrup J.; Immergut, E. H. *Polymer Handbook*; 3rd ed.; John Wiley & Sons: New York, 1989.
(25) Hashimoto, T.; Shibayama, M.; Kawai, H. *Macromolecules* **1980**, *13*, 1237.
(26) Hadziioannou, G.; Skoulios, A. *Macromolecules* **1982**, *15*, 258.
(27) Hashimoto, T.; Yamasaki, K.; Koizumi, S.; Hasegawa, H. *Macromolecules* **1993**, *26*, 2895.
(28) Prud'homme, J.; Perrier, M.; Denault, J. *Macromolecules* **1994**, *27*, 1493.
(29) Hashimoto, T.; Sakamoto, N. *Macromolecules* **1995**, *28*, 4779.
(30) Karatasos, K.; Anastasiadis, S. H.; Floudas, G.; Fytas, G.; Pispas, S.; Hadjichristidis, N.; Pakula, T. *Macromolecules* **1996**, *29*, 1326.
(31) Ishizu, K.; Fukuyama,T. *Macromolecules* **1989**, *22*, 244.
(32) Owens, J. N.; Gancarz, I. S.; Koberstein, J. T.; Russell, T. P. *Macromolecules* **1989**, *22*, 3380.
(33) Hashimoto, T.; Tanaka, H.; Hasegawa, H. *Macromolecules* **1990**, *23*, 4378.
(34) Tanaka, H.; Hasegawa, H.; Hashimoto, T. *Macromolecules* **1991**, *24*, 240.
(35) Winey, K. I.; Thomas, E. L.; Fetters, L. J. *Macromolecules* **1991**, *23*, 6182.
(36) Ehlich, D.; Takenaka, M.; Okamoto, S.; Hashimoto, T. *Macromolecules* **1993**, *26*, 189.
(37) Spontak, R. J.; Smith, S. D.; Ashraf; A. *Macromolecules* **1993**, *26*, 956.
(38) Balsara, N. P.; Lin, C. C.; Dai, H. J.; Krishnamoorti, R. *Macromolecules* **1994**, *25*, 3896.
(39) Winey, K. L.; Gobran, D. A.; Xu, Z.; Fetters, L. J.; Thomas, E. L. *Macromolecules* **1994**, *27*, 2392.
(40) Stühn, B.; Vilesov, A.; Zachmann, H. G. *Macromolecules* **1994**, *27*, 3560.
(41) Hajduk, D. A.; Harper, P. E.; Gruner, S. M.; Honeker, C. C.; Kim, G.; Thomas, E.L.; Fetters, L. J. *Macromolecules* **1994**, *27*, 4063.
(42) Okamoto, S.; Saijo, K.; Hashimoto, T. *Macromolecules* **1994**, *27*, 5547.
(43) Lin, C. C.; Jonnalagadda, S. V.; Kesani, P. K.; Dai, H. J.; Balsara, N. P. *Macromolecules* **1994**, *27*, 7769.
(44) Koizumi, S.; Hasegawa, H.; Hashimoto, T. *Macromolecules* **1994**, *27*, 7893.
(45) Kasten, H.; Stühn, B. *Macromolecules* **1995**, *28*, 4777.
(46) Mutter, R.; Stühn, B. *Macromolecules* **1995**, *28*, 5022.
(47) Han, C. D.; Baek, D. M.; Kim, J. K.; Ogawa, T.; Sakamoto, N.; Hashimoto, T. *Macromolecules* **1995**, *28*, 5043.
(48) Sakamoto, N.; Hashimoto, T. *Macromolecules* **1995**, *28*, 6825.
(49) Khandpur, A. K.; Förster, S.; Bates, F. S.; Hamley, I. W.; Ryan, A. J.; Bras, W.; Almdal, K.; Mortensen, K. *Macromolecules* **1995**, *28*, 8796.
(50) Ogawa; T.; Sakamoto, N.; Hashimoto, T.; Han, C. D.; Baek, D. M. *Macromolecules* **1996**, *29*, 2113.
(51) Matsushita, Y.; Mori, K.; Saguchi, R.; Nakao, Y.; Noda, I.; Nagasawa, M. *Macromolecules*, **1990**, *23*, 4313.
(52) Lin, H.; Steyerl, A.; Satija, S. K.; Karim, A.; Russell, T. P. *Macromolecules* **1995**, *28*, 1470.
(53) Russell, T. D.; Menelle, A.; Anastasiadis, S. H.; Satija, S. K.; Majkrzak, C. F. *Macromolecules* **1991**, *24*, 6263.
(54) Mayes, A. M.; Russell, T. P.; Satija, S. K.; Majkrzak, C. F. *Macromolecules* **1992**, *25*, 6523.
(55) Ryan, A. J.; Hamley, I. W.; Bras, W.; Bates, F. S. *Macromolecules* **1995**, *28*, 3860.
(56) Zhao, J.; Majumdar, B.; Schulz, M. F.; Bates, F. S.; Almdal, K.; Mortensen, K.; Hajduk, D. A.; Gruner, S. M. *Macromolecules* **1996**, *29*, 1204.
(57) Rosedale, J. H.; Bates, F. S.; Almdal, K.; Mortensen, K.; Wignall, G. D. *Macromolecules* **1995**, *28*, 1429.
(58) Grim, P. C. M.; Nyrkova, I. A.; Semenov, A. N.; ten Brinke, G.; Hadziioannou, G. *Macromolecules* **1995**, *28*, 7501.
(59) Jeon, K. J.; Roe R. J. *Macromolecules* **1994**, *27*, 2439.
(60) Gido, S. P.; Gunther, J.; Thomas, E. L.; Hoffman, D. *Macromolecules* **1993**, *26*, 4056.
(61) Floudas, G.; Fytas, G.; Hadjichristidis, N.; Pitsikalis, M. *Macromolecules* **1995**, *28*, 2359.
(62) Ghelsen, M. D.; Bates, F. S. *Macromolecules* **1994**, *27*, 3611.
(63) Jian, T.; Anastasiadis, S. H.; Semenov, A. N.; Fytas, G.; Adachi, K.; Kotaka, T. *Macromolecules* **1994**, *27*, 4762.
(64) Perahia, D.; Vacca, G.; Patel, S. S.; Dai, H. J.; Balsara; N. P. *Macromolecules* **1994**, *27*, 7645.
(65) Schuler, M.; Stühn, B. *Macromolecules* **1993**, *26*, 112.
(66) Sakurai, S.; Kawada, H.; Hashimoto, T.; Fetters, L. J. *Macromolecules* **1993**, *26*, 5796.
(67) Winey, K. I.; Thomas, E. L.; Fetters, L. J. *Macromolecules* **1992**, *25*, 2465.
(68) Hasegawa, H.; Tanaka, H.; Yamasaki, K.; Hashimoto, T. *Macromolecules* **1987**, *20*, 1651.
(69) Bühler, F.; Gronski, W. *Makromol. Chem.* **1986**, *187*, 2019.
(70) Winey, K. I.; Thomas, E. L.; Fetters, L. J. *J. Chem. Phys.* **1991**, *95*, 9367.

MA961261P